EEET ECOLOGICAL ENGINEERING & ENVIRONMENTAL TECHNOLOGY

Ecological Engineering & Environmental Technology, 2026, 27(12), 379–396
https://doi.org/10.12912/27197050/241685
ISSN 2719–7050, License CC-BY 4.0

Received: 2026.09.20
Accepted: 2026.10.21
Published: 2026.11.02

Spatio-temporal dynamics of mangrove cover based on Sentinel-2 imagery and Random Forest in Ketapang District, South Lampung, Indonesia

Apri Wijaya[1], Muhammad Kamal[2*], Prima Widayani[2]

[1] Master in Remote Sensing, Faculty of Geography, Universitas Gadjah Mada, Yogyakarta 55281, Indonesia
[2] Department of Geographic Information Science, Faculty of Geography, Universitas Gadjah Mada, Yogyakarta 55281, Indonesia
* Corresponding author's e-mail: m.kamal@ugm.ac.id

ABSTRACT

Mangrove forests fringe many tropical coastlines and provide important ecological and economic benefits, but they remain vulnerable to land conversion. This study analyzed the spatio-temporal dynamics of mangrove cover in Ketapang District, South Lampung Regency, Indonesia, between 2018 and 2026 using Sentinel-2 Level-2A imagery and a Random Forest (RF) classifier implemented in Google Earth Engine. Thirteen predictors were used: nine Sentinel-2 bands (B2, B3, B4, B5, B6, B7, B8, B11 and B12) and four spectral indices (NDVI, MNDWI, NDRE and NDTI). Five land cover classes (mangrove vegetation, non-mangrove vegetation, fish ponds, open land and water bodies) were mapped for 2018, 2020, 2022, 2024 and 2026. Against reference data interpreted from very-high-resolution imagery (2018–2024) and collected by field ground-truthing (2026), overall accuracy ranged from 91.79% to 96.34% and kappa from 0.89 to 0.95; error-adjusted areas with 95% confidence intervals were estimated from the error matrices. The SWIR-2 band (B12) had the highest Gini importance in every year. Mapped mangrove area increased from 196.64 ha in 2018 to 267.97 ha in 2026 (+71.33 ha), and the error-adjusted increase was 82.05 ± 13.42 ha. Decomposition of change showed that in 2018–2020 a small net change (+6.35 ha, within the classification uncertainty) was accompanied by a swap of 59.95 ha (30.48% of the 2018 mangrove area), whereas over the four intervals gross loss decreased from 29.97 to 18.88 ha and persistence increased from 84.76% to 92.70%. Overlay with the official rehabilitation sites (129.00 ha planted in 2020–2023) showed that the net increase occurred almost entirely within these sites (+80.83 ha, compared with −9.47 ha outside them) and that their share of the gross gain rose from 16.0% before the main planting to 58.3–77.5% in 2020–2024; this spatial association is consistent with a substantial contribution of rehabilitation planting, although causality was not tested. The results show how frequent Sentinel-2 mapping combined with transition analysis and uncertainty estimation can support the monitoring of mangrove rehabilitation.

Keywords: mangrove vegetation, Random Forest, rehabilitation, Sentinel-2, spatio-temporal dynamics

INTRODUCTION

Coastal wetlands are changing rapidly worldwide under pressure from human activities and climate change, and these changes have become a major concern for coastal management (Sharma et al., 2026; Thant et al., 2025). Mangrove ecosystems are essential for the health and productivity of coastal habitats (Akram et al., 2023). They play an important role in the global carbon cycle and in coastal protection: most of their carbon is stored in anoxic sediments where decomposition is slow, and they can store three to five times more carbon per hectare than terrestrial forests (Donato et al., 2011). Indonesia holds more than 2.9 million ha of mangroves, approximately 21% of the global total, and is therefore one of the largest reservoirs of coastal blue carbon (Murdiyarso et al., 2015).

Despite this, Indonesia has experienced substantial mangrove losses. Mangrove habitats continue to be fragmented and degraded through conversion to aquaculture, the construction of coastal infrastructure and other activities that alter coastal hydrology (Hagger et al., 2025; Zhao et al., 2026). The loss of mangroves also reduces the natural protection they provide against storm surges and tropical cyclones (Shokatianbeiragh et al., 2024). These pressures have led to a growing number of rehabilitation and restoration initiatives that aim to return degraded stands to their original structure, function and species composition (Lovelock et al., 2022; Mohan et al., 2024). According to the Ministry of Forestry of the Republic of Indonesia (MoF, 2025), Lampung Province has 10,797 ha of mangroves, of which approximately 450 ha are degraded.

Remote sensing overcomes many practical limitations of field surveys and allows effective, repeated and long-term monitoring of large coastal areas (Ghorbanian et al., 2021). Combined with GIS, it has been used for decades to monitor land cover change and shoreline dynamics in coastal zones and mangrove forests (Pham et al., 2019), and missions such as Landsat and Sentinel-2 enable the long-term monitoring of these ecosystems (Goldberg et al., 2020). The combination of Sentinel-2 imagery, spectral indices and a Random Forest (RF) classifier has repeatedly produced accurate mangrove maps and detailed descriptions of land cover transitions (Ahmad et al., 2023; Wang et al., 2025). However, most Indonesian studies of mangrove dynamics rely on only two or three observation dates that are irregularly spaced in time, for example in Batam (Aunurrahman et al., 2023), West Kalimantan (Widiastuti et al., 2024) and North Sumatra (Samsuri et al., 2026). Such sparse observations may miss short-term changes and spatial variations that become detectable when observations are more regularly distributed (Fallatah et al., 2026). A two-year interval is frequent enough to capture vegetation establishment and human activities, while limiting the influence of short-term seasonal variation.

Two further gaps limit the interpretation of such studies. First, most studies report only class areas and net change and ignore persistence, gross gain, gross loss and swap, although a small net change can conceal substantial turnover, for example mangrove loss in one place offset by gain elsewhere (Pontius et al., 2004). Second, mapped areas are rarely reported together with their uncertainty, although small changes may fall within the classification error (Olofsson et al., 2014). Separating the components of change and their uncertainty is relevant beyond description, because it indicates where interventions should be targeted and where rehabilitation zoning and the protection of eroding shorelines are needed (Goldberg et al., 2020; Su et al., 2021). Combining machine-learning classification with spatial transition analysis can therefore support conservation planning and the long-term provision of mangrove ecosystem services (Roy et al., 2025).

Ketapang District in South Lampung Regency, Indonesia, is a coastal area of strategic relevance: part of it is designated as a high-conservation-value zone under Indonesia's Forestry and Other Land Use (FOLU) Net Sink 2030 program (MoEF, 2022), and forest and land rehabilitation has been carried out along its coast. In Lampung Province, previous satellite-based studies have documented mangrove decline driven by fish-pond expansion (Kaskoyo et al., 2023), but no multi-date assessment of mangrove dynamics in Ketapang District is available. Compared with previous studies in Lampung and elsewhere in Indonesia, this study contributes (i) a consistent series of five Sentinel-2 maps at two-year intervals (2018–2026); (ii) the decomposition of mangrove change into persistence, gross gain, gross loss, net change and swap for each interval; and (iii) error-adjusted area estimates with 95% confidence intervals, which show which of the mapped changes exceed the classification uncertainty; and (iv) a comparison of mangrove change inside and outside the official rehabilitation sites. The processing scripts, reference samples and underlying calculations are provided as supplementary material to allow independent reproduction. The objectives of this research were (1) to map five land cover classes using Sentinel-2 spectral bands and indices and assess the classification accuracy and area uncertainty; and (2) to quantify mangrove transition components (persistence, gross gain, gross loss, net change and swap) for the four two-year intervals and relate them to the rehabilitation sites.

MATERIALS AND METHODS

Study site

This research was conducted in the coastal area of Ketapang District, South Lampung Regency, Lampung Province, Indonesia, located

at approximately 105°45′–105°55′E and 5°38′–5°50′S. The area of interest (AOI) was delineated as a buffer of approximately 300 m around the mangrove boundaries of the 2024 National Mangrove Map (MoF, 2025) and covers 1,047.37 ha. The buffer accommodates possible shifts of the mangrove boundary during 2018–2026 and includes the surrounding transition zones that may undergo land cover conversion. The research location is shown in Figure 1.

Data processing and analysis

Data collection and pre-processing

The overall research workflow is shown in Figure 2. The primary data were Sentinel-2 Level-2A (surface reflectance) images for 2018, 2020, 2022, 2024 and 2026, processed in Google Earth Engine (GEE). For 2020–2026, each image is a per-pixel median composite of all harmonized Sentinel-2A and Sentinel-2B Level-2A scenes that intersected the AOI (see Study Site) and were acquired between

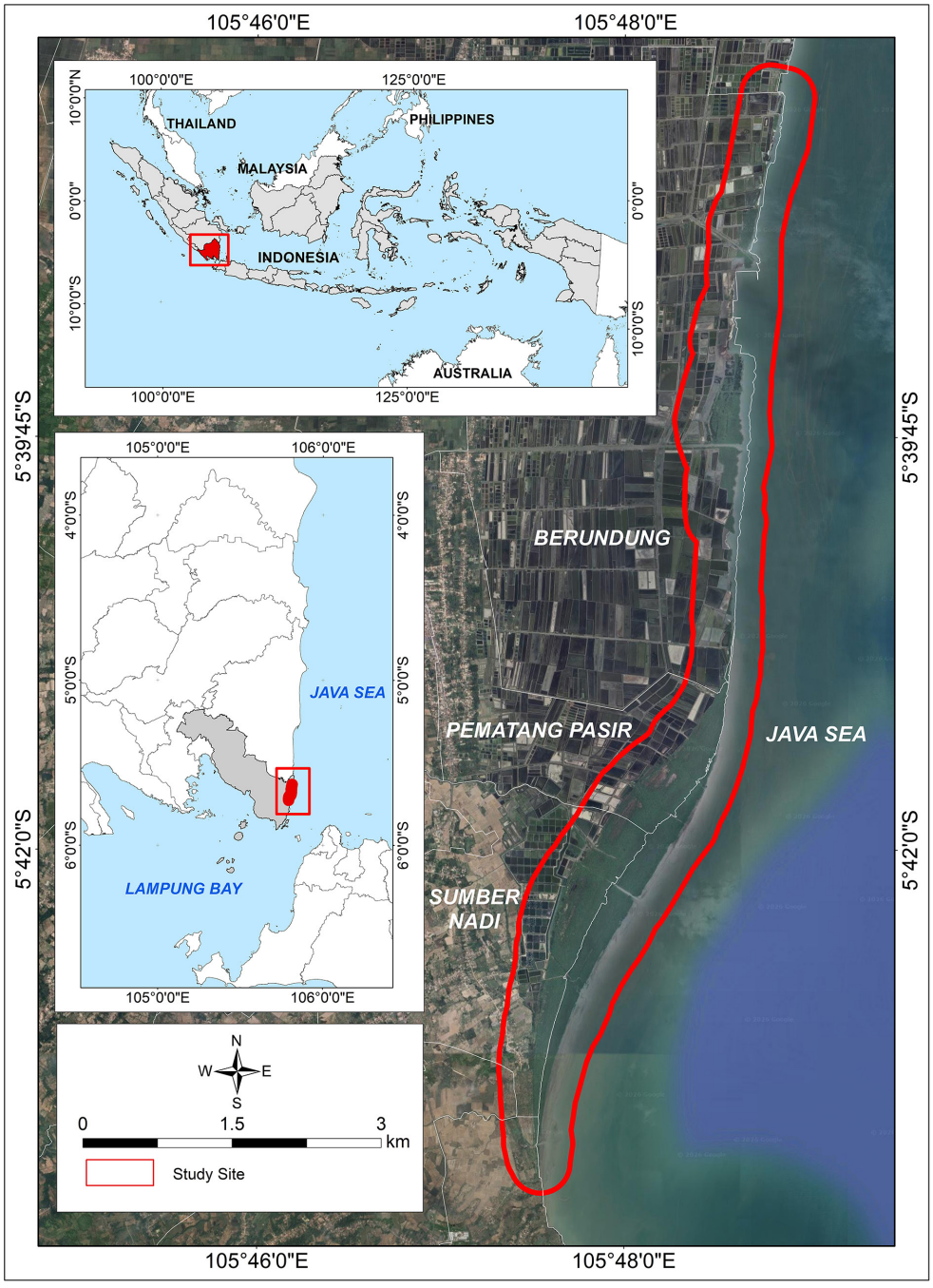

Figure 1. Study site in Ketapang District, South Lampung Regency, Lampung Province, Indonesia

1 June and 30 August; this dry-season window was used in every year to limit phenological, tidal and cloud-related differences between years. Scenes were pre-selected by scene-level cloud cover, and the remaining clouds were masked pixel by pixel with the s2cloudless cloud-probability product before compositing. Because cloud conditions differed between years, the cloud thresholds, cloud-shadow masking and gap filling were set for each year to obtain a complete, cloud-free composite of the AOI (Table 1). The 2026 composite was generated after 30 August 2026, when all scenes of the window were available. For 2018, the GEE catalogue contains no Level-2A scenes of the study area for the dry season, because Level-2A products were not generated systematically for this region before December 2018. A single Level-2A product acquired on 18 August 2018 (processing baseline 05.00; Table 1) was therefore downloaded from the Copernicus Data Space Ecosystem, its 20 m bands were resampled to 10 m by bilinear interpolation in QGIS, and the stacked image was uploaded to GEE. All images were converted to surface reflectance (digital number/10,000) and placed on a common 10 m grid (WGS 84/UTM zone 48S). For 2020–2026, the 20 m bands (B5, B6, B7, B11 and B12) were assigned to this grid by nearest-neighbor resampling (GEE default). Neither resampling method adds spatial detail, so the effective resolution of these bands remains 20 m. Overlay analysis and map layouts were produced in ArcMap 10.8 (Esri, Redlands, CA, USA), and accuracy and area statistics were tabulated in Microsoft Excel.

Spectral features and index transformation

Thirteen predictor variables were combined into one multiband dataset to improve the spectral separation of the land cover classes and to reduce spectral overlap between coastal land cover types. Nine are surface reflectance bands: the visible bands (B2, B3, B4), the red-edge bands (B5, B6, B7), the near-infrared band (B8) and the short-wave-infrared bands (B11, B12), selected for their sensitivity to chlorophyll content, canopy structure and moisture. The remaining four are spectral indices, whose formulas are given in Table 2.

Table 1. Sentinel-2 Level-2A input images and processing parameters of each year

Year	Source	Acquisition window	Scene cloud filter	Pixel-level cloud masking	Gap filling
2018	Single Level-2A product (CDSE)	18 Aug 2018	–	– (single date)	–
2020	GEE median composite	1 Jun–30 Aug 2020	≤ 10%	s2cloudless > 20%; cloud shadows; 50 m buffer	unmasked Jun–Aug median; Jun–Dec median; 7 × 7 focal mean
2022	GEE median composite	1 Jun–30 Aug 2022	< 60%	s2cloudless ≥ 40%	none
2024	GEE median composite	1 Jun–30 Aug 2024	≤ 60%	s2cloudless > 40%; cloud shadows; 100 m buffer; quality-band cloud flags	none
2026	GEE median composite	1 Jun–30 Aug 2026	< 60%	s2cloudless ≥ 40%	cloud-masked May–Aug 2026 median

Note: CDSE = Copernicus Data Space Ecosystem

Table 2. Spectral indices used as predictors

Spectral index	Formula	Function	Source
Normalized Difference Vegetation Index (NDVI)	(B8 − B4) / (B8 + B4)	Indicates the density and vigor of the vegetation canopy	Tucker & Sellers (1986)
Modified Normalized Difference Water Index (MNDWI)	(B3 − B11) / (B3 + B11)	Enhances open water and inundated fish ponds relative to land surfaces	Xu (2006)
Normalized Difference Red-Edge Index (NDRE)	(B8 − B5) / (B8 + B5)	Sensitive to chlorophyll content; improves the separation of mangroves from other vegetation	Gitelson & Merzlyak (1994)
Normalized Difference Turbidity Index (NDTI)	(B4 − B3) / (B4 + B3)	Increases with water turbidity and is also high for bright bare surfaces where red reflectance exceeds green reflectance; helps to distinguish turbid water and open land from vegetation and clear water	Lacaux et al. (2007)

Land cover classification

Five land cover classes were mapped: mangrove vegetation, non-mangrove vegetation, fish ponds, open land and water bodies. Training samples were polygons digitized for each class and year on the Sentinel-2 image of that year, supported by very-high-resolution imagery in Google Earth; all 10 m pixels within the polygons were used as training pixels. At least 30 training polygons were digitized for each class in each year. RF was implemented in GEE (ee.Classifier.smileRandomForest); the algorithm grows classification trees on bootstrap samples of the training pixels and assigns each pixel to the class that receives the majority of the tree votes. The hyperparameters were fixed a priori on the basis of the literature and were not tuned: number of trees (*ntree*) = 500, at which the accuracy of RF land cover classifications generally stabilizes (Belgiu & Dragut, 2016); number of predictors tested at each split (*mtry*) = 4, close to the square root of the 13 predictors (Breiman, 2001); minimum terminal-node size = 1 (GEE default); fraction of the training pixels used for each tree = 0.5 (GEE default); and a fixed random seed of 42. The same settings were used in all years.

The classification was carried out in two stages. First, a tentative model was trained on 70% of the training polygons of each class (stratified random split at the polygon level, seed 42) and checked on the remaining 30%; the split was made at the polygon level so that pixels of the same polygon were never used for both training and checking. The tentative map was used to check and, where necessary, revise the training polygons, and its classes served as strata for the validation sampling. Because this check relies on the same interpretation source as the training data, it is not independent, and its results are not reported as map accuracy; the validation samples were not used in this step. Second, the final model was trained on all training polygons and applied to the whole image.

The final maps were post-processed with a 3 × 3 majority filter and with rule-based corrections that address the confusion of fish ponds with open water: fish-pond pixels farther than 300 m from any land class, or farther than 500 m from vegetated land (NDVI > 0.15), were reassigned to water bodies; thin fish-pond strips removed by a morphological opening (radius of 2 pixels) and fish-pond patches smaller than 20 pixels (0.2 ha) were reassigned to water bodies (MNDWI > 0) or mangrove vegetation (MNDWI ≤ 0); and fish-pond pixels with more than 50% water bodies within a radius of 3 pixels were reassigned to water bodies. No manual editing was applied, and the same rules were used for all years.

Validation samples were points generated by stratified random sampling in ArcMap 10.8, with the classes of the tentative map of each year as strata. This design ensures that every class, including classes of small area, is represented by a sufficient number of samples, and it is recommended for accuracy assessment and area estimation (Olofsson et al., 2014). The points were placed at random within each class, independently of the training polygons, and their reference class was determined separately from the training data. Because the points were not generated outside the training polygons, an individual point could fall within a training polygon; such points were not removed, so that the random design was kept unchanged. For each class, the expected proportion of these points equals the proportion of the class area covered by training polygons. Each point corresponds to one 10 m pixel. For 2018–2024, the reference class of each point was determined by visual interpretation of historical very-high-resolution imagery in Google Earth Pro acquired within the June–August window of each year (12 June 2018, 27 July 2020, 21 July 2022 and 30 June 2024), i.e. in the same season as the Sentinel-2 images. The interpretation was based on visual keys of tone, color, texture, shape, size and context (e.g. dense, rough-textured canopy along the shoreline and creeks for mangrove vegetation; rectangular water-filled plots bounded by dikes for fish ponds; smooth dark surfaces for water bodies; and bright bare surfaces for open land). For 2026, the 270 points were visited during field ground-truthing between 10 and 30 June 2026, i.e. within the period covered by the 2026 composite. At each point, the dominant land cover of the surrounding homogeneous area was recorded, the position was measured with a handheld GPS receiver (positional accuracy better than 7 m), and photographs were taken. The number of validation points per class and year is reported with the accuracy results.

Accuracy assessment

The final maps were compared with the validation samples in a confusion matrix (rows:

reference class; columns: mapped class), from which user's accuracy (UA), producer's accuracy (PA), overall accuracy (OA) and the kappa coefficient were calculated. No accuracy threshold was used to accept or reject the final maps. Because class areas taken directly from a map are biased by classification errors, error-adjusted areas and their 95% confidence intervals were estimated with the stratified estimator of Olofsson et al. (2014), using the map classes as strata and the mapped area proportions as weights. The uncertainty of the change in mangrove area between two dates was approximated as $1.96 \times \sqrt{(SE_1^2 + SE_2^2)}$, where SE_1 and SE_2 are the standard errors of the two error-adjusted areas, and a change was considered to exceed the classification uncertainty when its 95% confidence interval did not include zero. Because the sampling strata were defined by the tentative map rather than by the final map, and the reference labels for 2018–2024

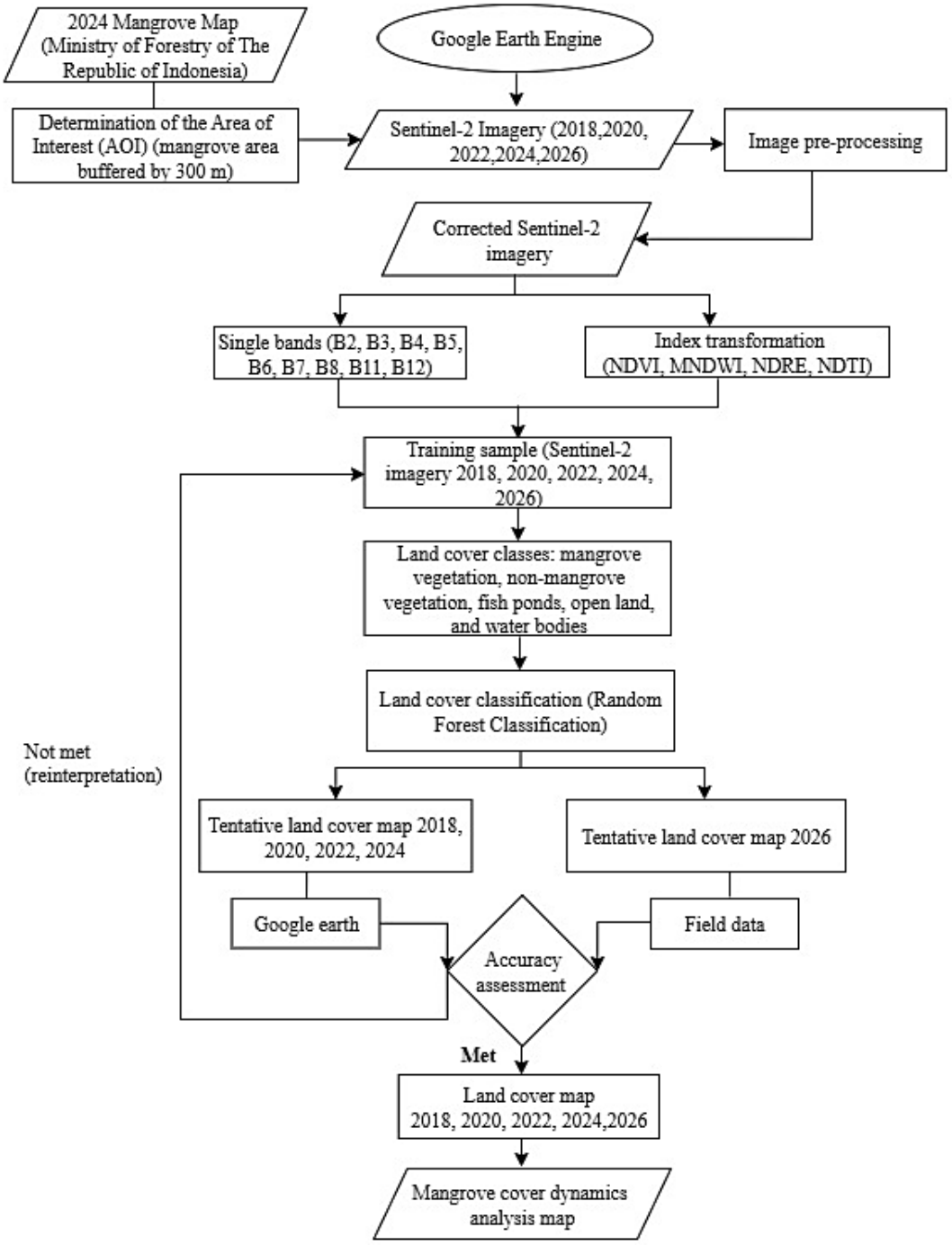

Figure 2. Research flow diagram

were interpreted from imagery, these confidence intervals should be regarded as approximate.

Mangrove transition analysis

The final maps of consecutive years were cross-tabulated in ArcMap 10.8 to obtain transition matrices of all classes for the four intervals 2018–2020, 2020–2022, 2022–2024 and 2024–2026. Following Pontius et al. (2004), mangrove change in each interval was decomposed into five components: persistence (area mapped as mangrove at both dates), gross gain (other classes converted to mangrove), gross loss (mangrove converted to other classes), net change (gross gain − gross loss) and swap (2 × the smaller of gross gain and gross loss). Swap quantifies change that occurs simultaneously as gain in some places and loss in others and therefore leaves the net area unchanged; a small net change can thus conceal considerable turnover. All components are expressed in hectares and as a percentage of the mangrove area at the start of the interval (e.g. swap in 2018–2020 = 59.95 ha / 196.64 ha = 30.48%). The transition components are based on mapped areas; their uncertainty is indicated by the error-adjusted area changes. To relate the mapped change to rehabilitation, the transition maps were overlaid (Identity tool, ArcMap 10.8) with the forest and land rehabilitation polygons of the Ministry of Forestry for 2020–2023, and persistence, gross gain and gross loss were summarized inside each rehabilitation site and outside the rehabilitation sites. The interval 2018–2020, which largely precedes the planting, served as a reference for the period before rehabilitation.

RESULTS AND DISCUSSION

Types and composition of mangrove vegetation

Four mangrove species were recorded during the 2026 field survey: *Avicennia marina*, *Rhizophora apiculata*, *Rhizophora stylosa* and *Rhizophora mucronata* (Figure 3). According to the forest and land rehabilitation spatial data of the Ministry of Forestry (Way Seputih Way Sekampung Watershed Management Center, BPDAS WSS), the *Rhizophora* stands originate from rehabilitation planting carried out in 2020–2023. *A. marina* is a pioneer species that can colonize newly formed mudflats and tolerate hypersaline conditions; its regeneration success and genetic structure depend mainly on tidal dynamics and distance from the shoreline (Triest et al., 2021). The three *Rhizophora* species look similar but can be distinguished by their leaves and propagules: *R. mucronata* has larger leaves and propagules, whereas *R. apiculata* and *R. stylosa* differ mainly in the color of the leaf tip, which is reddish in *R. stylosa* and green in *R. apiculata*. *R. apiculata* also has more prominent stilt roots and aerial roots, grows relatively quickly and is commonly used in rehabilitation planting. These species observations are qualitative; the spatial distribution and abundance of the species were not measured, and species composition was not mapped from the Sentinel-2 data.

Land cover classification

The RF classification mapped the five land cover classes in all five years (Figure 4), and the class areas are summarized in Figure 5. The maps reproduce the main landscape units of the study area: the mangrove belt along the shoreline and creeks, the fish-pond complex behind it, terrestrial vegetation further inland and open water.

Mapped mangrove area increased in every interval, from 196.64 ha in 2018 (18.77% of the study area) to 202.99 ha in 2020, 229.10 ha in 2022, 258.60 ha in 2024 and 267.97 ha (25.59%) in 2026, a mapped increase of 71.33 ha (36.27% of the 2018 area). The error-adjusted estimates (Table 3; Figure 6) confirm the increase over the whole period (82.05 ± 13.42 ha, 95% confidence interval) and in the intervals 2020–2022, 2022–2024 and 2024–2026, whereas the error-adjusted change in 2018–2020 (−5.06 ± 13.26 ha) does not differ from zero. The mapped expansion is consistent with mangrove establishment on accreting mudflats and in rehabilitation areas along this coast, and its spatial relationship with the rehabilitation sites is analyzed below.

Fish ponds showed the opposite trend. They were the most extensive class in 2018 (343.28 ha; 32.77%), decreased to 319.02 ha in 2020 and 298.90 ha in 2022, increased slightly to 305.65 ha in 2024 and decreased to 281.73 ha (26.90%) in 2026, a mapped decrease of 61.55 ha (17.93%). Conversion of fish ponds to mangrove accounted for 3.18, 9.82, 2.16 and 8.37 ha of mangrove

Figure 3. Dominant mangrove species observed in the study area: (a) *Avicennia marina*, (b) *Rhizophora apiculata*, (c) *Rhizophora stylosa* and (d) *Rhizophora mucronata*

gain in the four intervals, which suggests that some ponds were recolonized or replanted, as reported in other regions (Romañach et al., 2018); most of the decrease in fish ponds, however, was a transition to water bodies (84.49 ha in total). Water bodies, the largest class, varied between 413.86 and 460.67 ha. These fluctuations probably reflect differences in tidal stage and in pond water management between acquisition dates. Non-mangrove vegetation was relatively stable, increasing slightly from 63.91 to 69.17 ha. Open land increased from 0.28 ha in 2018 to 3.69 ha in 2026; because the class covers a small area, its error-adjusted area is highly uncertain.

Accuracy assessment of the Random Forest classification

The accuracy of the final maps of each year is summarized in Table 4. Overall accuracy ranged from 91.79% to 96.34% and kappa from 0.89 to 0.95 (Table 4), based on 270–355 validation points per year. For mangrove vegetation, PA ranged from 98.28% to 100% and UA from 92.05% to 100%; omission and commission errors of the mangrove class were therefore at most 1.72% and 7.95%, respectively. The area-weighted overall accuracy estimated following Olofsson et al. (2014) was slightly lower

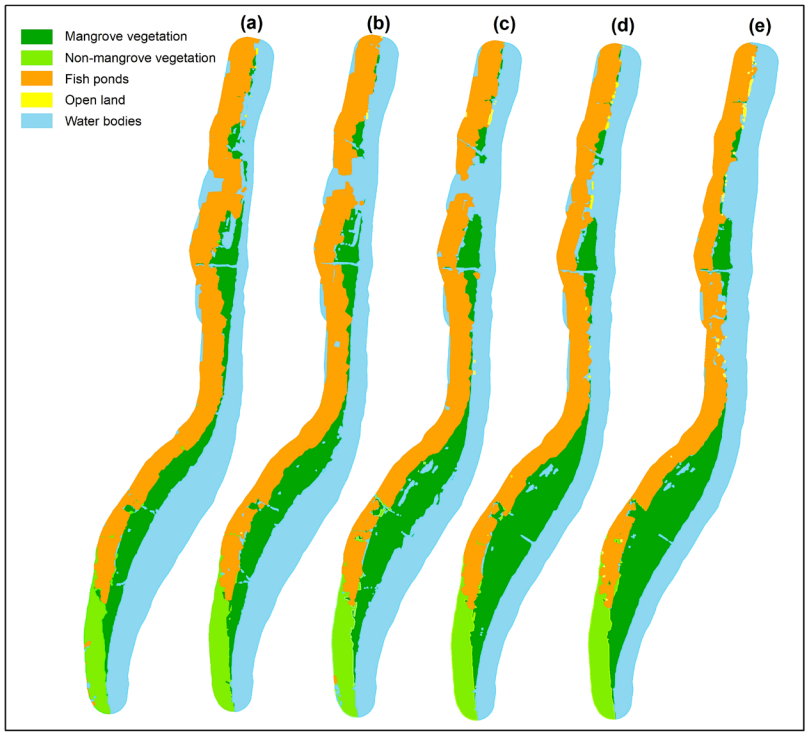

Figure 4. Land cover classification results for (a) 2018, (b) 2020, (c) 2022, (d) 2024 and (e) 2026

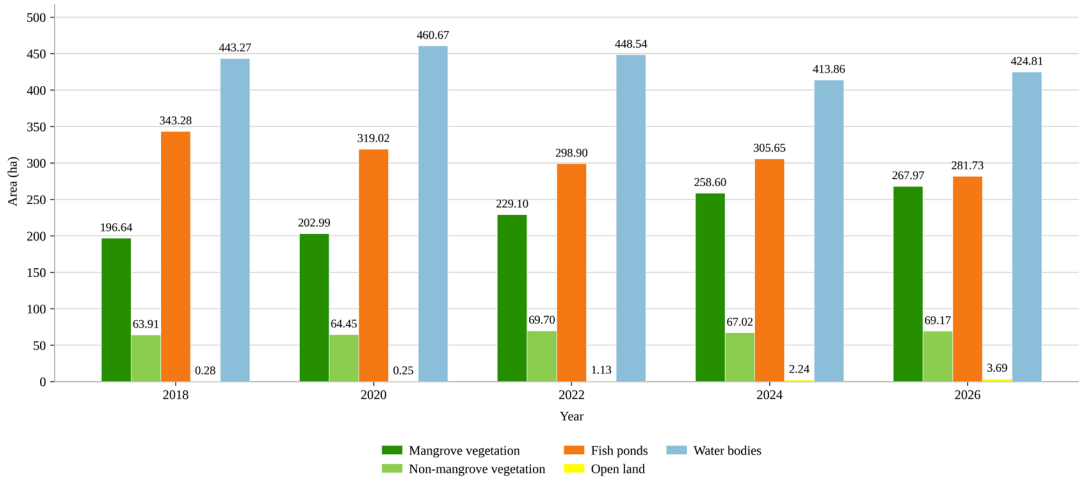

Figure 5. Area of the land cover classes, 2018–2026 (mapped areas)

(89.18–94.93%), because errors are weighted by the mapped area of each class.

Accuracy was lower for some of the other classes. Non-mangrove vegetation and fish ponds had PA and UA of at least 87% in all years. Water bodies had a high PA (93.59–100%) but a lower UA (80.22–90.80%): 9.20–19.78% of the points mapped as water belonged to other classes in the reference data, mainly fish ponds (for example, 9 and 11 fish-pond validation points were mapped as water in 2018 and 2020), because inundated ponds and turbid water are spectrally similar and pond water levels differ between acquisitions. Open land had a UA of 100% but a PA of only 70.00–83.33%, i.e. a substantial part of the open-land reference points was mapped as other classes, mostly as water bodies; the class covers a small area, its reference sample is small (24–43 points), and dry pond embankments resemble the surrounding bare soil. These errors are reflected in the error-adjusted areas, which indicate that

Table 3. Mapped and error-adjusted mangrove area and area change with 95% confidence intervals (CI), 2018–2026

Year / period	Mapped (ha)	Error-adjusted (ha)	95% CI (± ha)	Change exceeds uncertainty
Area				
2018	196.64	191.91	6.53	–
2020	202.99	186.84	11.54	–
2022	229.10	227.11	9.70	–
2024	258.60	249.69	9.97	–
2026	267.97	273.95	11.73	–
Change				
2018–2020	+6.35	−5.06	13.26	No
2020–2022	+26.11	+40.27	15.08	Yes
2022–2024	+29.51	+22.57	13.91	Yes
2024–2026	+9.37	+24.27	15.39	Yes
2018–2026	+71.33	+82.05	13.42	Yes

Note: Error-adjusted areas follow the stratified estimator of Olofsson et al. (2014); the CI of a change is $1.96 \times \sqrt{(SE_1^2 + SE_2^2)}$.

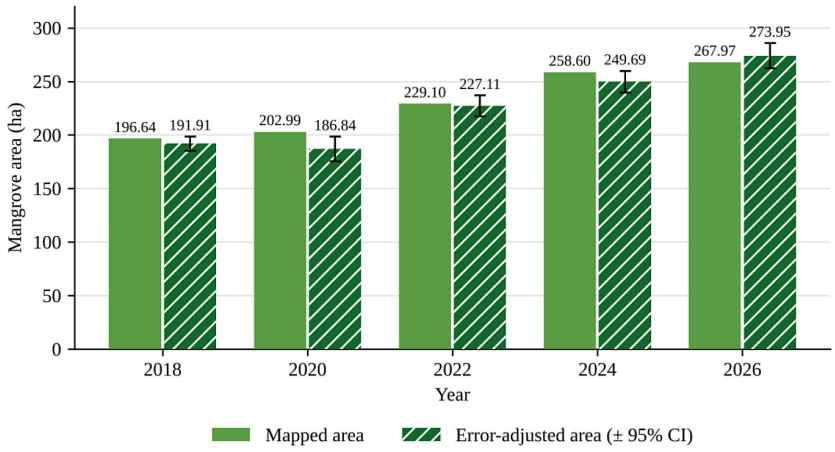

Figure 6. Mapped and error-adjusted mangrove area (± 95% confidence interval), 2018–2026

water bodies were overestimated and fish ponds and open land underestimated in the maps.

RF is a non-parametric ensemble classifier that handles high-dimensional multispectral data well and is relatively robust to correlated predictors (Belgiu & Dragut, 2016), although correlation between predictors affects the interpretation of variable importance (see below). The large number of trees stabilizes the ensemble prediction, and the random selection of four predictors at each split reduces the correlation between the trees of the ensemble (Maxwell et al., 2018).

Analysis of variable contribution

The contribution of each predictor was evaluated with the variable importance of the final RF model of each year, expressed as the mean decrease in Gini impurity. Figure 7 shows the importance of the 13 predictors in each year.

The SWIR-2 band (B12) ranked first in all five years (mean importance 1,523.20), and the SWIR-1 band (B11) ranked second in four of the five years (mean 1,364.58), followed by B5 (1,313.88) and MNDWI (1,301.88). The SWIR region (1.56–2.20 µm) is sensitive to the moisture of the canopy and of the substrate (D. Wang et al., 2018), which is relevant in a coastal setting where mangrove canopies, inundated ponds and estuarine water are otherwise difficult to separate; in addition, water absorbs SWIR radiation strongly (Bunting et al., 2018).

The red-edge bands B5 (1,313.88) and B7 (1,293.86) also had high importance, in line with

Table 4. Accuracy of the Random Forest classification, 2018–2026 (n = number of validation points of the reference class)

Year	Land cover class	n	Producer's accuracy (PA, %)	User's accuracy (UA, %)	Overall accuracy (OA, %)	Kappa coefficient (κ)
2018	Mangrove vegetation	81	100.00	97.59	93.55	0.92
	Non-mangrove vegetation	52	98.08	92.73		
	Water bodies	78	100.00	82.98		
	Fish ponds	100	88.00	100.00		
	Open land	30	70.00	100.00		
2020	Mangrove vegetation	81	100.00	92.05	91.79	0.89
	Non-mangrove vegetation	52	96.15	96.15		
	Water bodies	78	93.59	80.22		
	Fish ponds	100	87.00	98.86		
	Open land	30	73.33	100.00		
2022	Mangrove vegetation	86	98.84	97.70	93.64	0.92
	Non-mangrove vegetation	56	92.86	100.00		
	Water bodies	79	100.00	82.29		
	Fish ponds	101	87.13	96.70		
	Open land	24	83.33	100.00		
2024	Mangrove vegetation	84	100.00	96.55	96.34	0.95
	Non-mangrove vegetation	56	96.43	100.00		
	Water bodies	80	98.75	90.80		
	Fish ponds	101	96.04	97.98		
	Open land	34	82.35	100.00		
2026	Mangrove vegetation	58	98.28	100.00	95.19	0.94
	Non-mangrove vegetation	56	100.00	98.25		
	Water bodies	62	100.00	87.32		
	Fish ponds	51	92.16	94.00		
	Open land	43	81.40	100.00		

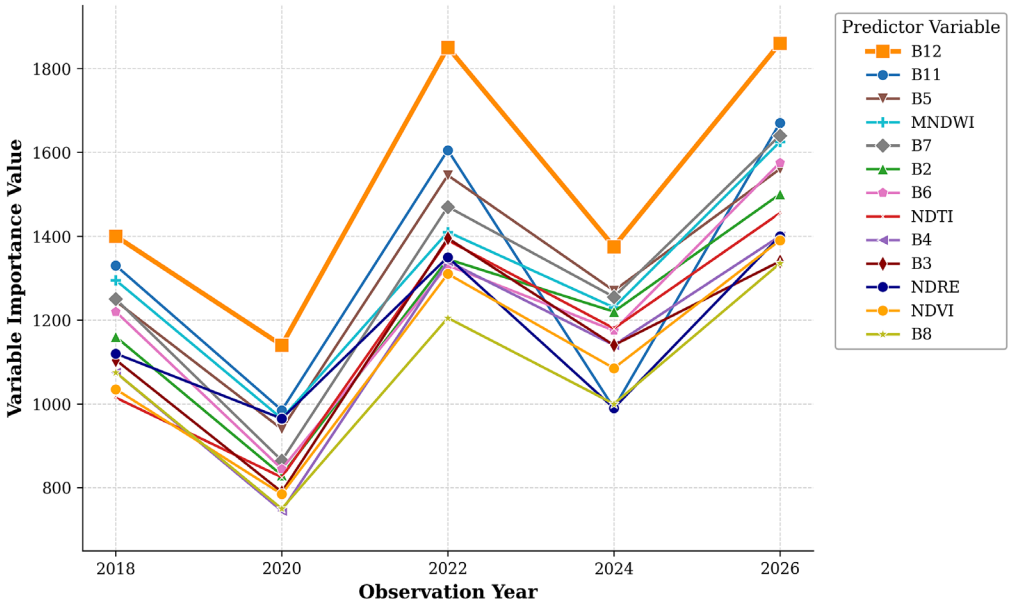

Figure 7. Variable importance (mean decrease in Gini impurity) of the 13 predictors in the RF models, 2018–2026

the sensitivity of the red-edge region (690–780 nm) to chlorophyll absorption and leaf structure, which helps to separate dense mangrove canopies, where broad visible and near-infrared bands tend to saturate, from inland vegetation (Poursanidis et al., 2019). Apart from MNDWI, the indices had intermediate importance: NDTI (1,159.44), NDRE (1,132.04) and NDVI (1,122.34). The importance of NDTI may reflect its high values for both turbid water and bright bare surfaces (Lacaux et al., 2007), which may help to distinguish these surfaces from vegetation and clear water.

These importance values should be interpreted with caution. Gini importance measures how much a predictor contributes to node purity in the fitted trees; it is not a measure of the physical effect of the variable. When predictors are correlated, as here, where the indices are computed from the same bands (e.g. NDVI from B8 and B4, and MNDWI from B3 and B11), importance can be shared among them, and a predictor may appear less important because a correlated predictor was selected instead (Strobl et al., 2007). The absolute values also depend on the training sample of each year and are therefore compared through ranks. With these caveats, the consistent first rank of B12 indicates that SWIR information was the most useful for separating the classes in this setting.

Mangrove transition dynamics

Figure 8 shows the spatial pattern of mangrove persistence, gain and loss in each interval, Figure 9 the transition components in hectares, and Table 5 the components in hectares and as a percentage of the mangrove area at the start of each interval.

In 2018–2020, the net change was small (+6.35 ha; 3.23% of the 2018 mangrove area), but it resulted from a gross gain of 36.32 ha and a gross loss of 29.97 ha, giving a swap of 59.95 ha (30.48% of the 2018 mangrove area; Table 5). The largest exchange was with water bodies: 31.65 ha of water became mangrove and 24.03 ha of mangrove became water. Part of this exchange probably occurred along the seaward and creek edges of the mangrove, where mixed pixels, differences in tidal stage between acquisitions and the use of a single-date image in 2018 can produce apparent change; this is consistent with the error-adjusted change for 2018–2020, which does not differ from zero (Table 3). A small net change can thus conceal considerable spatial turnover, and observations several years apart (e.g. five to ten years) may miss such short-term dynamics (Joe et al., 2026). In the following intervals, gross loss decreased from 29.97 ha (15.24%) to 18.88 ha (7.30%), swap decreased from 30.48% to 14.60%, and persistence increased from 84.76% to 92.70% (Table 5).

The lower gross loss and swap and the higher persistence in the later intervals indicate that the mapped mangrove extent became spatially more stable after 2020. Possible explanations include the trapping of fine sediment by expanding mangrove root systems and the attenuation of wave energy, which may stabilize previously eroding margins; however, these processes were not measured in this study and should be tested with field measurements of sedimentation and shoreline change. Regardless of the causes, the results show that frequent monitoring and transition components (gross gain, gross loss and swap) reveal where mangrove extent changes, information that net area alone does not provide and that is useful for planning conservation and coastal risk-reduction measures.

Comparison with other studies

The mapped increase of 36.27% in Ketapang contrasts with trends reported elsewhere. In West Kalimantan (Widiastuti et al., 2024) and North Sumatra (Samsuri et al., 2026), deforestation pressure on mangrove cover was reported to persist, and Fallatah et al. (2026) show that coastal degradation remains widespread in many tropical regions. Within Lampung Province, Kaskoyo et al. (2023) reported a substantial decrease in mangrove cover in Tulang Bawang Regency, mainly due to the expansion of fish ponds. Unlike these studies, which mainly report net change between dates, the present results show that the net increase in Ketapang was accompanied by considerable spatial turnover in the first interval and by increasing persistence afterwards. Differences in sensors, class definitions, periods and accuracy reporting limit direct comparison, but the contrast suggests that local conditions, such as sediment supply, the availability of abandoned ponds and rehabilitation activities, strongly influence mangrove trajectories.

(a)

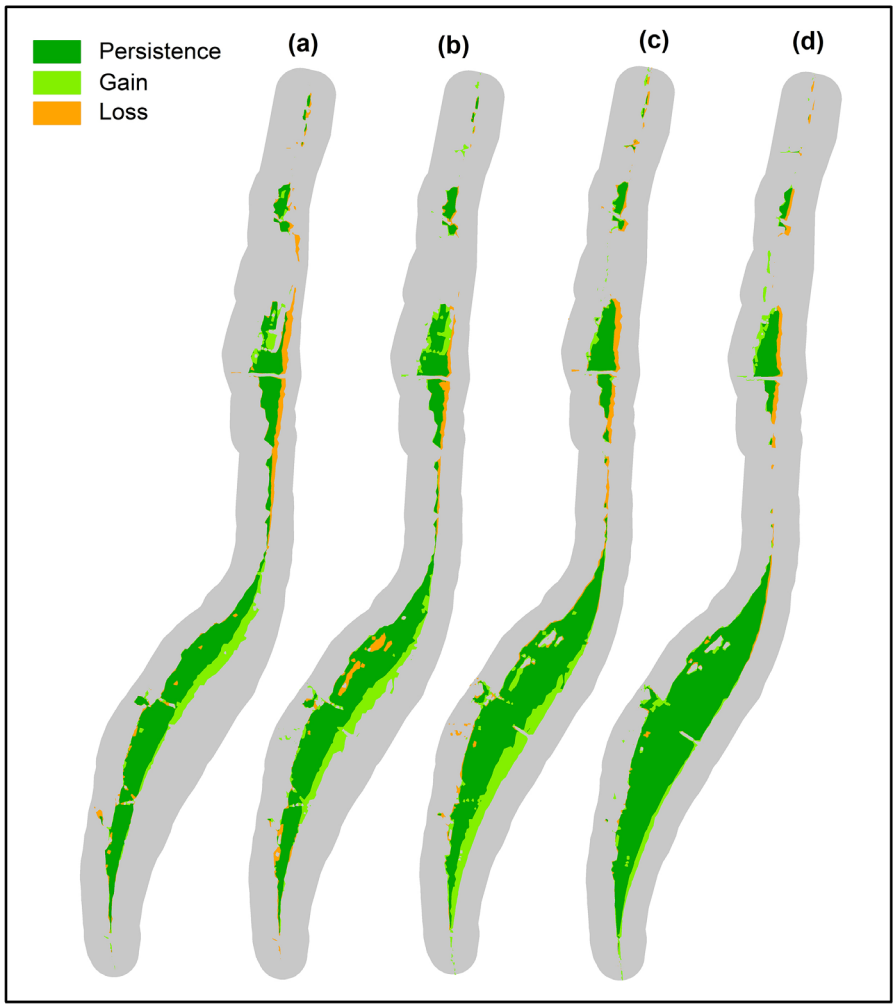

(b)

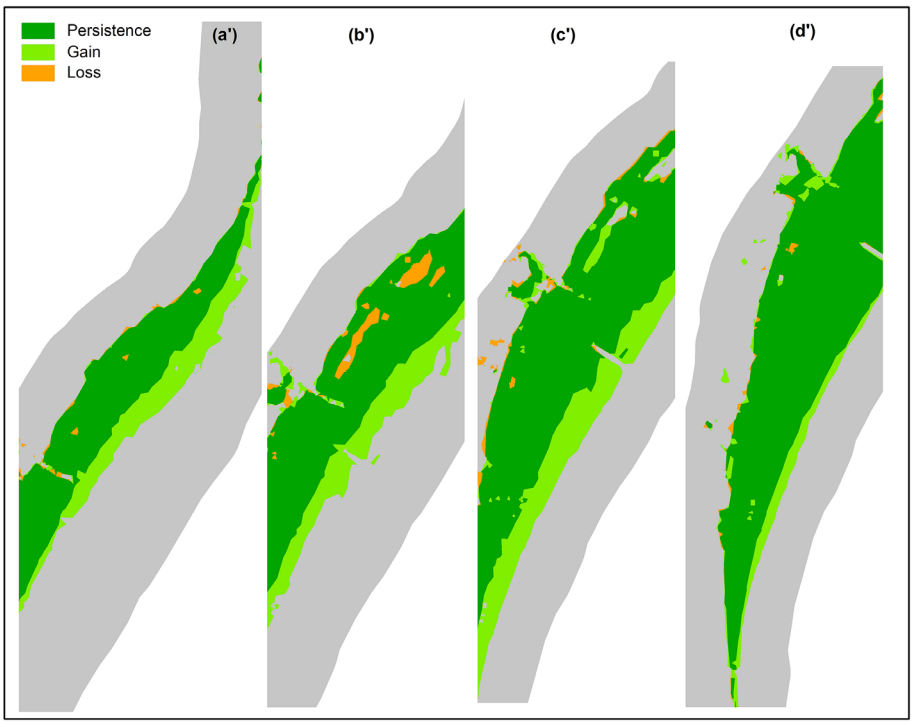

Figure 8. Spatial pattern of mangrove persistence, gain and loss for (a) 2018–2020, (b) 2020–2022, (c) 2022–2024 and (d) 2024–2026, with enlarged views of the same intervals in (a′)–(d′)

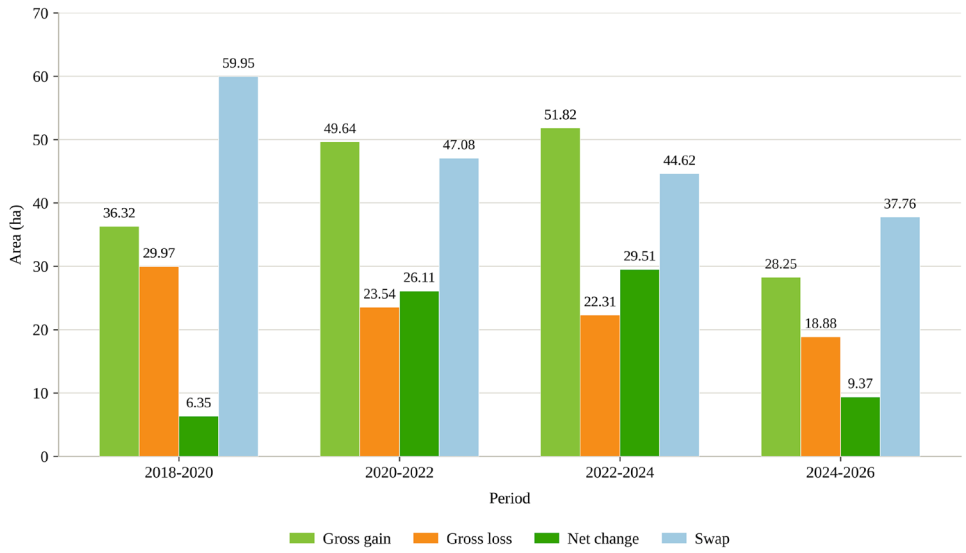

Figure 9. Mangrove transition components (gross gain, gross loss, net change and swap, ha) for the four intervals, 2018–2026

Table 5. Components of mangrove change per interval, in ha and, in parentheses, as a percentage of the mangrove area at the start of the interval

Component	2018–2020	2020–2022	2022–2024	2024–2026
Mangrove at start (ha)	196.64	202.99	229.10	258.60
Persistence	166.67 (84.76)	179.45 (88.40)	206.79 (90.26)	239.72 (92.70)
Gross gain	36.32 (18.47)	49.64 (24.46)	51.82 (22.62)	28.25 (10.92)
Gross loss	29.97 (15.24)	23.54 (11.60)	22.31 (9.74)	18.88 (7.30)
Net change	+6.35 (3.23)	+26.11 (12.86)	+29.51 (12.88)	+9.37 (3.62)
Swap	59.95 (30.48)	47.08 (23.19)	44.62 (19.48)	37.76 (14.60)
Total change	66.29 (33.71)	73.18 (36.05)	74.13 (32.36)	47.13 (18.22)
Mangrove at end (ha)	202.99	229.10	258.60	267.97

Note: net change = gross gain − gross loss; swap = 2 × min(gross gain, gross loss); total change = net change + swap. Percentages refer to the mangrove area at the start of each interval.

Possible drivers of mangrove gain – natural colonization and rehabilitation

The causes of the mapped mangrove gain were not tested experimentally, and the following interpretation is based on the spatial association between the gain and the rehabilitation sites. According to the rehabilitation spatial data of the Ministry of Forestry, rehabilitation planting within the study area covered 129.00 ha in 2020–2023 (106.98 ha in 2020, 5.25 ha in 2021, 10.00 ha in 2022 and 6.77 ha in 2023), i.e. 12.3% of the AOI, mainly along the seaward fringe (Figure 10). In 2018–2020, which largely precedes the planting, these sites accounted for 16.0% of the gross gain (5.79 of 36.32 ha), close to their share of the AOI. After planting, their share rose to 58.3% in 2020–2022 (28.94 ha), 77.5% in 2022–2024 (40.17 ha) and 37.4% in 2024–2026 (10.56 ha) (Table 6). Within the rehabilitation sites, the mapped mangrove area increased from 5.85 ha in 2018 to 86.68 ha in 2026 (+80.83 ha), whereas outside them it decreased slightly from 190.79 to 181.32 ha (−9.47 ha); the net increase in the AOI therefore occurred within the rehabilitation sites, while the area outside them showed a small net loss. The 2020 sites, which contained almost no mangrove in 2018 (1.9% of their area), were 69.6% mangrove in 2026, and their largest gains occurred two to four years after planting, consistent with the time needed for seedlings to form a canopy that is detectable at 10–20 m resolution. By contrast, the 2021 site was already 72.6% mangrove in 2018, which indicates enrichment planting within existing stands, and changed

little. Nearly all gain within the rehabilitation sites (97.0%) came from areas mapped as water bodies at the start of the interval, i.e. intertidal mudflats along the seaward fringe.

Tarigan et al. (2020) reported active sedimentation along the eastern coast of South Lampung, with suspended sediment supplied by nearby river estuaries and mud particle sizes of 0.0258–0.0330 mm, which may have provided a suitable substrate for both planting and natural establishment (no hydro-oceanographic measurements were made in the present study). Pioneer species such as A. marina have been reported to colonize newly formed mudflats in other regions (Fallatah et al., 2026; Joe et al., 2026), but the present data do not allow the species involved in the mapped gain to be identified. The spatial association does not establish causality: the planting sites may have been selected on accreting mudflats where natural colonization would also have occurred, no unplanted control sites were analyzed, and part of the gain from water may reflect differences in tidal stage and mixed pixels at the water edge (see above). Field comparisons of planted and unplanted mudflats and measurements of sedimentation are needed to separate the effect of planting from natural colonization.

Limitations

Several limitations should be considered. First, the 2018 image is a single-date product whose 20 m bands were resampled by bilinear interpolation, and the compositing parameters of the 2020–2026 composites differ between years (Table 1); some of the mapped change, particularly at the land–water interface, may therefore reflect differences in image conditions rather than land cover change. Second, the validation points were stratified by the classes of the tentative map rather than of the final map, and the reference data for 2018–2024 were interpreted from imagery rather than collected in the field, so the confidence intervals of the error-adjusted areas are approximate. In addition, the validation points were generated without excluding the areas of the training polygons, so some of them may coincide with training pixels; this would make the reported accuracies slightly optimistic, particularly for classes whose area is largely covered by training polygons. Third, the 20 m bands limit the detection of narrow mangrove fringes, and species composition, stand structure and biomass cannot be derived from the classification. Finally, the relationship between rehabilitation and mangrove

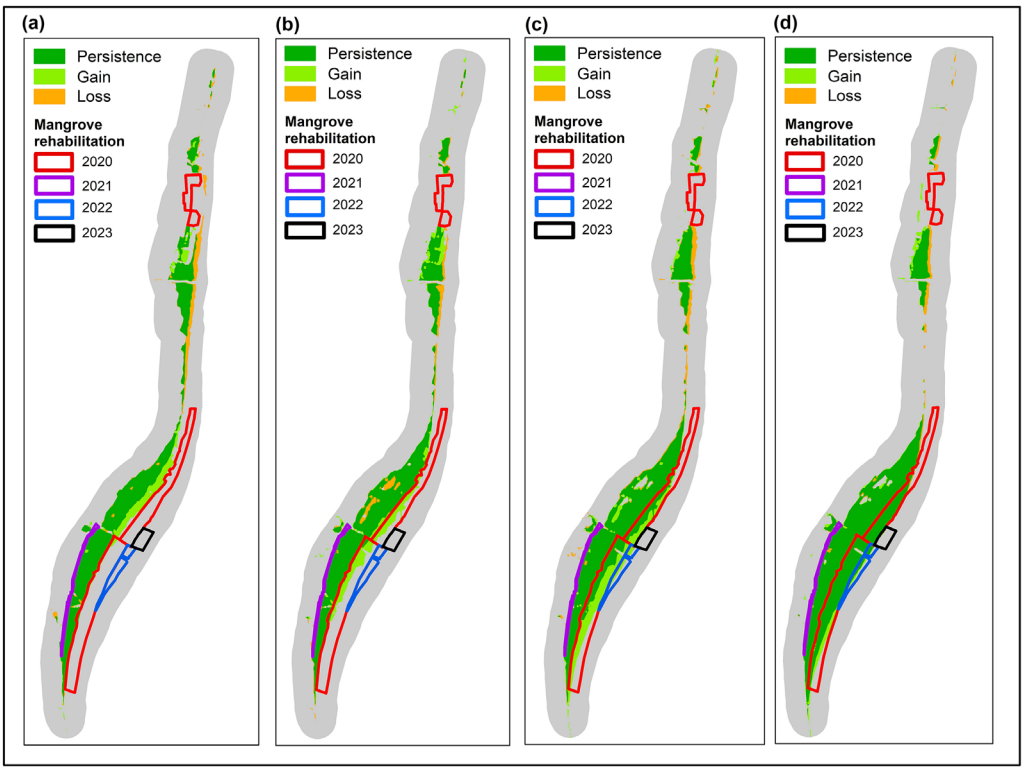

Figure 10. Spatial pattern of mangrove persistence, gain and loss for (a) 2018–2020, (b) 2020–2022, (c) 2022–2024 and (d) 2024–2026, overlaid with the mangrove rehabilitation sites of 2020–2023

Table 6. Gross mangrove gain and net change inside and outside the rehabilitation sites per interval (mapped areas, ha)

Interval	Gross gain inside rehabilitation sites (ha)	Gross gain outside rehabilitation sites (ha)	Share of gross gain inside (%)	Net change inside (ha)	Net change outside (ha)
2018–2020	5.79	30.53	16.0	+4.56	+1.79
2020–2022	28.94	20.71	58.3	+27.42	−1.32
2022–2024	40.17	11.68	77.5	+39.33	−9.79
2024–2026	10.56	17.69	37.4	+9.53	−0.16
2018–2026	85.46	80.61	51.5	+80.83	−9.47

gain is based on the spatial association with the planting sites rather than on a controlled comparison, and sedimentation was not measured.

CONCLUSIONS

Multitemporal Sentinel-2 data classified with Random Forest in Google Earth Engine allowed mangrove cover in Ketapang District, South Lampung Regency, Indonesia, to be mapped at two-year intervals between 2018 and 2026. With 13 spectral predictors, overall accuracy ranged from 91.79% to 96.34% and kappa from 0.89 to 0.95; the producer's and user's accuracies of the mangrove class were at least 98.28% and 92.05%, respectively, whereas water bodies (UA 80.22–90.80%) and open land (PA 70.00–83.33%) were mapped less accurately. The SWIR-2 band (B12) had the highest Gini importance in every year, although the importance of correlated predictors should be interpreted with caution. Mapped mangrove area increased from 196.64 ha in 2018 to 267.97 ha in 2026 (+71.33 ha; +36.27%), and the error-adjusted increase of 82.05 ± 13.42 ha shows that this increase exceeds the classification uncertainty. This is an increase in mangrove cover; changes in stand structure, biomass, species composition and ecosystem functions were not assessed.

The transition analysis revealed dynamics that net area alone does not show: in 2018–2020, a small net change (+6.35 ha, within the classification uncertainty) concealed a swap of 59.95 ha (30.48% of the 2018 mangrove area), whereas in the following intervals gross loss decreased and persistence increased to 92.70%, indicating a spatially more stable mangrove extent. The net increase occurred almost entirely within the official rehabilitation sites planted in 2020–2023 (+80.83 ha inside versus −9.47 ha outside), whose share of the gross gain rose from 16.0% before planting to 58.3–77.5% in 2020–2024, which is consistent with a substantial contribution of rehabilitation planting on accreting mudflats. Because no unplanted control sites were analyzed, this result represents a spatial association rather than a demonstrated causal effect.

Acknowledgments

The authors would like to express their gratitude to the Faculty of Geography, Universitas Gadjah Mada, for its collaboration with the Ministry of Forestry of the Republic of Indonesia in providing research funding through Indonesia's FOLU Net Sink 2030 program. The authors also extend their appreciation to the Way Seputih Way Sekampung Watershed Management Center (BPDAS), the Lampung Provincial Forestry Office, and the local community of Ketapang District for their administrative support and assistance during field data collection.

REFERENCES

1. Ahmad, H., Abdallah, M., Jose, F., Eldin, H., Bhuyan, S., James, D., & Selvam, S. (2023). Evaluation and mapping of predicted future land use changes using hybrid models in a coastal area. *Ecological Informatics*, *78*, 102324. https://doi.org/10.1016/j.ecoinf.2023.102324
2. Akram, H., Hussain, S., Mazumdar, P., Chua, K. O., Butt, T. E., & Harikrishna, J. A. (2023). Mangrove health: a review of functions, threats, and challenges associated with mangrove management practices. *Forests*, *14*(9), 1698. https://doi.org/10.3390/f14091698
3. Aunurrahman, Anggoro, S., Muskananfola, M. A. X. R., & Saputra, S. (2023). Detection and analysis of mangrove cover change in Kepalajerih Island, Batam, Indonesia using Landsat Imagery. *Biodiversitas*, *24*(11), 6126–6133. https://doi.org/10.13057/biodiv/d241134

4. Belgiu, M., & Dragut, L. (2016). Random forest in remote sensing: A review of applications and future directions. *ISPRS Journal of Photogrammetry and Remote Sensing*, *114*, 24–31. https://doi.org/10.1016/j.isprsjprs.2016.01.011
5. Breiman, L. (2001). Random Forests. *Machine Learning*, *45*(1), 5–32. https://doi.org/10.1023/A:1010933404324
6. Bunting, P., Rosenqvist, A., Lucas, R. M., Rebelo, L., Hilarides, L., Thomas, N., Hardy, A., Itoh, T., Shimada, M., & Finlayson, C. M. (2018). The global mangrove watch-A new 2010 global baseline of mangrove extent. *Remote Sensing*, *10*(10), 1669. https://doi.org/10.3390/rs10101669
7. Donato, D. C., Kauffman, J. B., Murdiyarso, D., Kurnianto, S., Stidham, M., & Kanninen, M. (2011). Mangroves among the most carbon-rich forests in the tropics. *Nature Geoscience*, *4*(5), 293–297. https://doi.org/10.1038/ngeo1123
8. Fallatah, A., Alattas, A., Habibullah, A., Mandourah, A., Sahahiri, R., Baik, A., Alshawabkeh, Y., & Elfleet, M. (2026). Monitoring mangrove deforestation using Google Earth Engine and Random Forest Machine Learning Algorithm. *Land*, *15*(6), 901. https://doi.org/10.3390/land15060901
9. Ghorbanian, A., Zaghian, S., Asiyabi, R. M., Amani, M., Mohammadzadeh, A., & Jamali, S. (2021). Mangrove ecosystem mapping using Sentinel-1 and Sentinel-2 satellite images and Random Forest Algorithm in Google Earth Engine. *Remote Sensing*, *13*(13), 2565. https://doi.org/10.3390/rs13132565
10. Gitelson, A. A., & Merzlyak, M. N. (1994). Spectral reflectance changes associated with autumn senescence of Aesculus hippocastanum L. and Acer platanoides L. leaves. Spectral features and relation to chlorophyll estimation. *Journal of Plant Physiology*, *143*(3), 286–292. https://doi.org/10.1016/S0176-1617(11)81633-0
11. Goldberg, L., Lagomasino, D., Thomas, N., & Fatoyinbo, T. (2020). Global declines in human-driven mangrove loss. *Global Change Biology*, *26*(10), 5844–5855. https://doi.org/10.1111/gcb.15275
12. Hagger, V., Vanderklift, M. A., Beaumont, K. P., Olds, A., Dittman, S., & Lovelock, C. E. (2025). Biodiversity gains can be achieved with coastal wetland restoration for plants, invertebrates, birds, and bats. *Ecological Indicators*, *178*, 113805. https://doi.org/10.1016/j.ecolind.2025.113805
13. Joe, R. J. J., Pitchaimani, V. S., Dhanalakshmi, S., Abishek, S. R., Alosanai, A. A., & Karuppannan, S. (2026). Assessment of coastal land use land cover transitions and ecological degradation in Thiruvananthapuram, India using machine learning. *Estuarine, Coastal and Shelf Science*, *340*, 110020. https://doi.org/10.1016/j.ecss.2026.110020
14. Kaskoyo, H., Hartati, F., Bakri, S., & Febryano, I. G. (2023). Satellite based analysis of mangrove cover and density change in mangroves of Tulang Bawang District, Lampung Province, Indonesia. *Biodiversitas*, *24*(5), 3019–3028. https://doi.org/10.13057/biodiv/d240557
15. Lacaux, J.-P., Tourre, Y. M., Vignolles, C., Ndione, J.-A., & Lafaye, M. (2007). Classification of ponds from high-spatial resolution remote sensing: Application to Rift Valley Fever epidemics in Senegal. *Remote Sensing of Environment*, *106*(1), 66–74. https://doi.org/10.1016/j.rse.2006.07.012
16. Lovelock, C. E., Barbier, E., & Duarte, C. M. (2022). Tackling the mangrove restoration challenge. PLoS Biology, 20(10), e3001836. https://doi.org/10.1371/journal.pbio.3001836
17. Maxwell, A. E., Warner, T. A., & Fang, F. (2018). Implementation of machine-learning classification in remote sensing: an applied review. *International Journal of Remote Sensing*, *39*(9), 2784–2817. https://doi.org/10.1080/01431161.2018.1433343
18. MoEF. (2022). *Operational Plan of Indonesia's FOLU Net Sink 2030 Sub-National Lampung Province (Report No. A-17/Renja-Lampung/09/2022)*. Ministry of Environment and Forestry of the Republic of Indonesia. (in Indonesian)
19. MoF. (2025). *National Mangrove Map 2024 (Decree of the Minister of Forestry of the Republic of Indonesia No. 594/2025)*. (in Indonesian)
20. Mohan, M., Dutta Roy, A., Montenegro, J. F., Watt, M. S., Burt, J. A., Shapiro, A., Ouerfelli, D., Daniel, R., de-Miguel, S., Ali, T., Ortega Pardo, M., Al Sayah, M., Aboobacker, V. M., El Beyrouthy, N., Reef, R., Adrah, E., AlMealla, R., Pitumpe Arachchige, P. S., Selvam, P., . . . Chambers, J. Q. (2024). Mangrove forest regeneration age map and drivers of restoration success in Gulf Cooperation Council countries from satellite imagery. *Remote Sensing Applications: Society and Environment*, *36*, 101345. https://doi.org/10.1016/j.rsase.2024.101345
21. Murdiyarso, D., Purbopuspito, J., Kauffman, J. B., Warren, M. W., Sasmito, S. D., Donato, D. C., Manuri, S., Krisnawati, H., Taberima, S., & Kurnianto, S. (2015). The potential of Indonesian mangrove forests for global climate change mitigation. *Nature Climate Change*, *5*(12), 1089–1092. https://doi.org/10.1038/nclimate2734
22. Olofsson, P., Foody, G. M., Herold, M., Stehman, S. V., Woodcock, C. E., & Wulder, M. A. (2014). Good practices for estimating area and assessing accuracy of land change. *Remote Sensing of Environment*, *148*, 42–57. https://doi.org/10.1016/j.rse.2014.02.015
23. Pham, T. D., Yokoya, N., Bui, D. T., & Yoshino, K. (2019). Remote sensing approaches for monitoring mangrove species, structure, and biomass: Opportunities and challenges. *Remote Sensing*, *11*(3), 230. https://doi.org/10.3390/rs11030230

24. Pontius, R. G., Shusas, E., & McEachern, M. (2004). Detecting important categorical land changes while accounting for persistence. *Agriculture, Ecosystems and Environment*, *101*(2–3), 251–268. https://doi.org/10.1016/j.agee.2003.09.008
25. Poursanidis, D., Traganos, D., Reinartz, P., & Chrysoulakis, N. (2019). On the use of Sentinel-2 for coastal habitat mapping and satellite-derived bathymetry estimation using downscaled coastal aerosol band. *International Journal of Applied Earth Observation and Geoinformation, 80*, 58–70. https://doi.org/10.1016/j.jag.2019.03.012
26. Romañach, S. S., DeAngelis, D. L., Koh, H. L., Li, Y., Teh, S. Y., Raja Barizan, R. S., & Zhai, L. (2018). Conservation and restoration of mangroves: Global status, perspectives, and prognosis. *Ocean and Coastal Management*, *154*, 72–82. https://doi.org/10.1016/j.ocecoaman.2018.01.009
27. Roy, S. K., Mojumder, P., Arman, A., & Hasan, M. (2025). Evaluating mangrove forest dynamics and fragmentation in Sundarbans, Bangladesh using high-resolution Sentinel-2 satellite images. *Global Ecology and Conservation*, *58*, e03493. https://doi.org/10.1016/j.gecco.2025.e03493
28. Samsuri, Zaitunah, A., Amaliah, N., Sulitioadi, Y., & Duryat. (2026). Mangrove cover and shoreline changes detection using multi-temporal Landsat Imagery and Digital Shoreline Analysis System (DSAS) in Labuhanbatu Regency, Indonesia. *Jurnal Sylva Lestari*, *14*(1), 160–178. https://doi.org/10.23960/jsl.v14i1.1259
29. Sharma, J., Raju, B., & Mahtab, A. (2026). Spatio-temporal dynamics in Bhitarkanika mangroves amid climate change showcasing the resilience and vulnerability due to cyclonic events. *Next Sustainability*, *7*, 100233. https://doi.org/10.1016/j.nxsust.2025.100233
30. Shokatianbeiragh, M., Banan-Dallalian, M., Golshani, A., Allahadadi, M., & Samiee-Zenoozian, M. (2024). The effectiveness of mangrove forests as a nature-based solution against flood risk under an extreme weather event. *Regional Studies in Marine Science*, *77*, 103630. https://doi.org/10.1016/j.rsma.2024.103630
31. Strobl, C., Boulesteix, A., Zeileis, A., & Hothorn, T. (2007). Bias in random forest variable importance measures: Illustrations, sources and a solution. *BMC Bioinformatics*, *8*(1), 25. https://doi.org/10.1186/1471-2105-8-25
32. Su, J., Friess, D. A., & Gasparatos, A. (2021). A meta-analysis of the ecological and economic outcomes of mangrove restoration. *Nature Communications*, *12*, 5050. https://doi.org/10.1038/s41467-021-25349-1
33. Tarigan, T., Simarmata, N., & Nurisman, N. (2020). Analysis of sediment and its impact on shoreline conditions in the eastern coastal area of South Lampung Regency. *Journal of Science and Applicative Technology*, *4*(1), 26–31. https://doi.org/10.35472/jsat.v4i1.249. (in Indonesian)
34. Thant, P., Dai, Z., Mei, X., An, B., & Van, C. M. (2025). Machine learning-based detection of changes in mapping the mangrove forest of the Yangon estuary, Southeast Asia. *Marine Environmental Research*, *210*, 107343. https://doi.org/10.1016/j.marenvres.2025.107343
35. Triest, L., Socorro, A., Gado, V. J., Mazo, A. M., & Sierens, T. (2021). Avicennia genetic diversity and fine-scaled structure influenced by coastal proximity of mangrove fragments. *Frontiers in Marine Science*, *8*, 643982. https://doi.org/10.3389/fmars.2021.643982
36. Tucker, C. J., & Sellers, P. J. (1986). Satellite remote sensing of primary production. *International Journal of Remote Sensing*, *7*(11), 1395–1416. https://doi.org/10.1080/01431168608948944
37. Wang, D., Wan, B., Qiu, P., Su, Y., Guo, Q., Wang, R., Sun, F., & Wu, X. (2018). Evaluating the performance of Sentinel-2, Landsat 8 and Pléiades-1 in mapping mangrove extent and species. *Remote Sensing*, *10*(9), 1468. https://doi.org/10.3390/rs10091468
38. Wang, S., Chen, T., Li, Z., & Sang, H. (2025). Fine monitoring method for mangrove wetland ecosystem based on sentinel data fusion and RF optimization. *Systems and Soft Computing*, *7*, 200376. https://doi.org/10.1016/j.sasc.2025.200376
39. Widiastuti, T., Astiani, D., Roslinda, E., Ekyastuti, W., & Ekamawanti, H. (2024). Mangrove land cover changes in North Singkawang, West Kalimantan, Indonesia analyzed using Landsat 8 images. *Biodiversitas*, *25*(9), 3160–3167. https://doi.org/10.13057/biodiv/d250938
40. Xu, H. (2006). Modification of Normalised Difference Water Index (NDWI) to enhance open water features in remotely sensed imagery. *International Journal of Remote Sensing*, *27*(14), 3025–3033. https://doi.org/10.1080/01431160600589179
41. Zhao, B., Dai, Z., Xiong, Y., Long, C., Mei, X., & Cheng, J. (2026). From degradation to conservation: Tracking mangrove dynamic changes of Hainan Island in China. *Journal of Environmental Management*, *405*, 129639. https://doi.org/10.1016/j.jenvman.2026.129639